



# Inflammasome-Mediated Neuronal-Microglial Crosstalk: a Therapeutic Substrate for the Familial *C9orf72* Variant of Frontotemporal Dementia/Amyotrophic Lateral Sclerosis

Kyle J. Trageser<sup>1</sup> · Eun-Jeong Yang<sup>1</sup> · Chad Smith<sup>1</sup> · Ruth Iban-Arias<sup>1</sup> · Tatsunori Oguchi<sup>1</sup> · Maria Sebastian-Valverde<sup>1</sup> · Umar Haris Iqbal<sup>1</sup> · Henry Wu<sup>1</sup> · Molly Estill<sup>2</sup> · Md Al Rahim<sup>1</sup> · Urdhva Raval<sup>1</sup> · Francis J. Herman<sup>1</sup> · Yong Jie Zhang<sup>3</sup> · Leonard Petrucelli<sup>3</sup> · Giulio Maria Pasinetti<sup>1,4</sup>

Received: 10 January 2023 / Accepted: 12 March 2023 / Published online: 3 April 2023

This is a U.S. Government work and not under copyright protection in the US; foreign copyright protection may apply 2023

## Abstract

Intronic G<sub>4</sub>C<sub>2</sub> hexanucleotide repeat expansions (HRE) of *C9orf72* are the most common cause of familial variants of frontotemporal dementia/amyotrophic lateral sclerosis (FTD/ALS). G<sub>4</sub>C<sub>2</sub> HREs in *C9orf72* undergo non-canonical repeat-associated translation, producing dipeptide repeat (DPR) proteins, with various deleterious impacts on cellular homeostasis. While five different DPRs are produced, poly(glycine-arginine) (GR) is amongst the most toxic and is the only DPR to accumulate in the associated clinically relevant anatomical locations of the brain. Previous work has demonstrated the profound effects of a poly (GR) model of *C9orf72* FTD/ALS, including motor impairment, memory deficits, neurodegeneration, and neuroinflammation. Neuroinflammation is hypothesized to be a driving factor in the disease course; microglia activation is present prior to symptom onset and persists throughout the disease. Here, using an established mouse model of *C9orf72* FTD/ALS, we investigate the contributions of the nod-like receptor pyrin-containing 3 (NLRP3) inflammasome in the pathogenesis of FTD/ALS. We find that inflammasome-mediated neuroinflammation is increased with microglial activation, cleavage of caspase-1, production of IL-1 $\beta$ , and upregulation of *Cxcl10* in the brain of *C9orf72* FTD/ALS mice. Excitingly, we find that genetic ablation of *Nlrp3* significantly improved survival, protected behavioral deficits, and prevented neurodegeneration suggesting a novel mechanism involving HRE-mediated induction of innate immunity. The findings provide experimental evidence of the integral role of HRE in inflammasome-mediated innate immunity in the *C9orf72* variant of FTD/ALS pathogenesis and suggest the NLRP3 inflammasome as a therapeutic target.

**Keywords** Amyotrophic lateral sclerosis · Frontotemporal dementia · Microglia · *C9orf72* · Neuroinflammation · Neurodegeneration · Inflammasome

## Introduction

Amyotrophic lateral sclerosis (ALS) is a progressive neurodegenerative disorder in which patients exhibit selective loss and demyelination of corticospinal motor neurons leading to terminal motor function impairments [1]. The pathophysiology underlying ALS is poorly characterized, which leaves patients with limited therapeutic options. ALS may have a familial or sporadic etiology; the most prevalent monogenic cause of familial ALS is G<sub>4</sub>C<sub>2</sub> repeat expansions in chromosome 9 open reading frame 72 (*C9orf72*). *C9orf72*-ALS has a high concomitant rate of diagnosis with frontotemporal dementia (FTD), a neurodegenerative disease presenting with behavioral and cognitive impairments [2]. Intronic G<sub>4</sub>C<sub>2</sub> hexanucleotide repeat expansions (HREs)

Kyle J. Trageser and Eun-Jeong Yang are co-first authors.

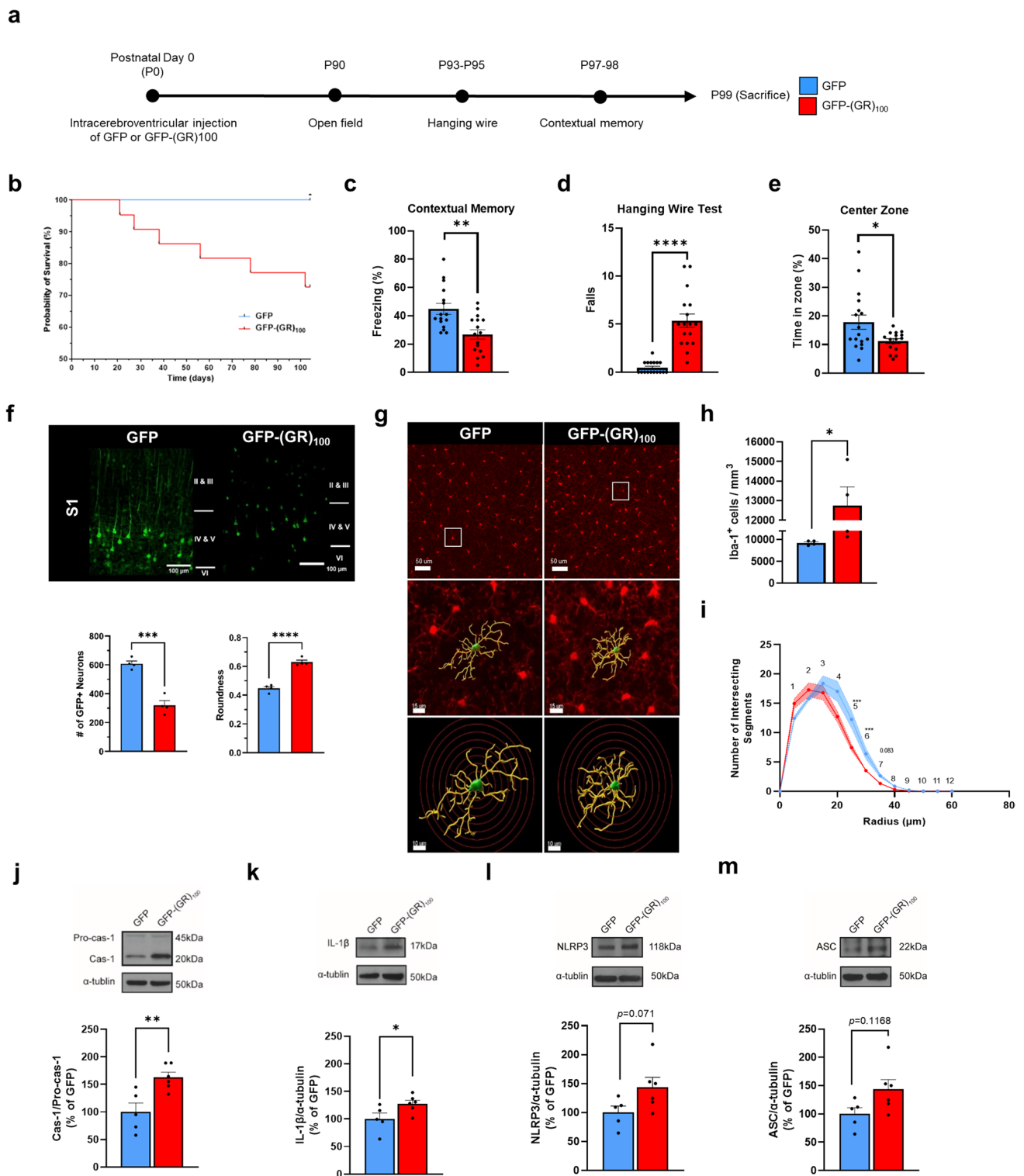
✉ Giulio Maria Pasinetti  
giulio.pasinetti@mssm.edu

<sup>1</sup> Department of Neurology, Icahn School of Medicine at Mount Sinai, New York, NY 10029, USA

<sup>2</sup> Department of Neuroscience, Icahn School of Medicine at Mount Sinai, New York, NY 10029, USA

<sup>3</sup> Department of Neuroscience, Mayo Clinic, Jacksonville, FL 32224, USA

<sup>4</sup> Geriatric Research, Education and Clinical Center, James J. Peters Veterans Affairs Medical Center, Bronx, NY 10468, USA



of *C9orf72* are the most common feature of the *C9orf72* familial variants of FTD/ALS resulting in the generation of several neurotoxic dipeptide repeat (DPR) proteins [3]. Most importantly, the poly (glycine-arginine) (GR) is amongst the most toxic and the primary DPR to accumulate in susceptible brain regions undergoing degeneration in the brain of

ALS/FTD subjects [4]. Recent evidence strongly supports the pathogenetic role of poly (GR) in *C9orf72* FTD/ALS, including motor impairment, memory deficits, neurodegeneration, and neuroinflammation [5, 6].

The high rate of concurrent diagnosis of FTD and ALS and the ongoing investigation into overlapping

**Fig. 1** Innate immune-driven neuroinflammation and neurodegeneration in a GFP-(GR)<sub>100</sub> model of *C9orf72* FTD/ALS. **a** Graphical illustration of the workflow process. **b** Probability of survival of GFP and GFP-(GR)<sub>100</sub>. The probability of survival was analyzed by log-rank test. **c** Freezing in contextual fear memory task. **d** Number of falls on the third day of the hanging wire test. **e** Time spent in the central zone in the open field test (\* $p < 0.05$ ; \*\* $p < 0.01$ ; \*\*\*\* $p < 0.0001$ , compared to GFP mice,  $n = 16$ – $17$  mice for each group). **f** Representative GFP and GFP-(GR)<sub>100</sub>-expression neurons in the layers of IV and V of S1 cortical region. Green: GFP and GFP-(GR)<sub>100</sub>. Length bar, 100  $\mu\text{m}$ . Bar graph showing the count (lower left panel) and somatic roundness (lower right panel) of GFP- and GFP-(GR)<sub>100</sub>-expression neurons in the S1 cortical region. **g** Representative immunohistochemical images showing Iba-1 immunopositive cells (upper panel) and 3D reconstruction of Iba-1 immunopositive cells in the S1 cortical region, with increasing radii in 5  $\mu\text{m}$  steps to measure branch intersections (middle and lower panels). The outline with a white box in the upper panel is magnified in the middle and lower panels. Length bars, 50  $\mu\text{m}$ , 15  $\mu\text{m}$ , and 10  $\mu\text{m}$  in the upper, middle, and lower panels, respectively. Red: Iba-1 immunostaining. Green: Soma. Yellow: branches. **h** Microglial density in the S1 cortical region. **i** Sholl analysis of microglia in S1 cortical region (\* $p < 0.05$ ; \*\*\*\* $p < 0.0001$ , compared to GFP mice,  $n = 4$  mice for each group). **j** Representative bands (upper panel) and densitometric quantification of the ratio of active caspase-1 to pro-caspase-1 (lower panel) in the cerebral cortex, normalized to GFP. **k** Representative bands (upper panel) and densitometric quantification of cleaved IL-1 $\beta$  in the cerebral cortex (lower panel), normalized to GFP. **l** Representative bands (upper panel) and densitometric quantification of NLRP3 in the cerebral cortex (lower panel), normalized to GFP. **m** Representative bands (upper panel) and densitometric quantification of NLRP3 in the cerebral cortex (lower panel), normalized to GFP (\* $p < 0.05$ ; \*\* $p < 0.01$ ; compared to GFP mice,  $n = 5$ – $6$  mice for each group). **c–m** were analyzed by unpaired  $t$ -test. Data are presented as mean  $\pm$  SEM

pathomechanisms have led to the notion of an FTD/ALS neurodegenerative spectrum disorder [7]. Recent investigations into the pathogenesis of ALS find that dysregulated innate immune activity may act as a detrimental mechanism that affects neuronal structure and function in line with our findings [8]. Our previous study suggests that activation of innate immunity in our model system [9] is highly relevant for its deleterious effect in promoting neuroinflammation through a mechanism involving pro-inflammatory cascades in the brain, as also described in other neurodegenerative conditions [10–12]. For example, since neuronal stress is a common feature in other forms of FTD/ALS, our evidence provides the basis for the broad therapeutic translatability in other forms of ALS, including SOD1<sup>G93A</sup> and TDP-43.

Here, we find evidence suggesting a potential new mechanism by which neuronal stress is induced by DPR proteins in the *C9orf72* variant of FTD/ALS. Most importantly, we find that silencing *Nlrp3*-mediated innate immunity significantly attenuates mortality and neurodegeneration and most notably mitigates behavioral impairments. Collectively, our study adds critical information toward understanding the etiology and pathogenesis of the familial *C9orf72* variant of FTD/ALS implicating novel mechanisms involving

chemokine-mediated activation of the NLRP3 inflammasome-mediated innate immunity as a therapeutic target for the *C9orf72* variant of FTD/ALS.

## Materials and Methods

### Reagents and Mice

The AAV<sub>9</sub>-GFP and AAV<sub>9</sub>-GFP-(GR)<sub>100</sub> viruses were a kind gift from Dr. Leonard Petrucelli. Unless specified otherwise, cell culture reagents were obtained from Thermo Fisher Scientific (Waltham, MA) and antibodies were obtained from Abcam (Cambridge, MA). C57BL/6J WT mice (#000664) and *Nlrp3*<sup>-/-</sup> mice (#021302) were obtained from The Jackson Laboratory (Bar Harbor, ME) and socially housed on a 12:12-h light/dark cycle with lights on at 07:00 h in a temperature-controlled (20  $\pm$  2  $^{\circ}\text{C}$ ) vivarium. For *Nlrp3*<sup>-/-</sup> genotyping, the primers were used (mutant forward; 5'-TGC CTGCTCTTTACTGAAGG-3', WT forward; 5'-TCAGTT TCCTTGCTACCAGA-3', and common reverse; 5'-TTC CATTACAGTCACTCCAGATGT-3') [13]. Mice were given food and water ad libitum and were bred to obtain mouse pups used in our studies. All experiments in this study were performed using both female and male mice. The animals were randomly assigned to different experimental groups, and care was taken to ensure an equal representation of both sexes in each group. All procedures were approved by the Institutional Animal Care and Use Committee of the Icahn School of Medicine at Mount Sinai.

### *C9orf72* Experimental Model

Upon confirmation of pregnancy, WT and *Nlrp3*<sup>-/-</sup> dames were separated and monitored daily for litters. After the identification of a milk spot to confirm that newborn (p0) pups were being nursed, the pups were injected with AAV<sub>9</sub>-GFP or AAV<sub>9</sub>-GFP-(GR)<sub>100</sub> by the ICV method (Fig. 1a) [14]. Pups were cryoanesthetized by placing them in a padded 15-mL tube partially submerged in a slurry of water and crushed ice. Upon confirmation of anesthesia by toe-pinch, we identified the point of injection, approximately two-fifths of the distance between bregma and each eye. A Hamilton syringe (#7634-01; Reno, NV) with a 32-gauge needle (10 mm long, Hamilton #7803-04) was loaded with 4  $\mu\text{L}$  of the AAV vector and placed 2 mm deep, orthogonal to the mouse's head at the point of injection. A total of 2  $\mu\text{L}$  of the AAV vector was injected at a rate of 1  $\mu\text{L}$  min into each lateral ventricle [15]. Upon completion of injections, each pup was rapidly returned to physiological temperatures by placing on a warming pad. The litters were returned to dames upon completion of injection for the entire litter and monitored for acceptance. Mice were weaned at p30 by sex.

For confirmation of diffusion prior to studies, a small number of mice were injected with Trypan Blue and sacrificed 2 h later for dissection of the brain and examination by stereoscopic microscope.

## Behavioral Testing

After reaching 3 months of age, mice were tested through a battery of behavioral tests (Fig. 1a). All behavioral testing took place during the light phase of the day. On all days of behavioral testing, mice were acclimated to an anteroom directly adjacent to the behavioral testing room for 30 min. On day 1, mice were tested in the open field test for basal anxiety and general locomotor impairments [16]. The open field apparatus consisted of a 40 cm × 40 cm × 40 cm Plexiglas box with opaque white walls, situated within a dimly lit room (200 lux). Mice were placed in the center of the apparatus and were allowed to freely explore for 10 min before being returned to their home cage. On day 3 through 5, mice were tested in a hanging wire test for muscular impairments [17]. The hanging wire apparatus consisted of a 2-mm-thick wire suspended 35 cm over a layer of corn cob bedding, situated in a brightly lit room (500 lux). Mice were lifted from their home cage by the base of their tail and were placed near the wire until they grasped it with their forelimbs. The number of falls over a 2-min period was recorded. Falls in which the mice hung from the wire from their hindlimbs were excluded from the number of falls. At the end of the behavioral trial, mice were returned to their home cages. On days 7 through 9, mice were tested in a contextual and cued memory test in two contexts. Context A was a 30 cm × 24 cm × 21 cm conditioning chamber (Med Associates, Fairfax VT) within a room with white walls and bright lighting. Context A had a bare metal grid floor, bare gray walls, bright lighting, and background fan noise. Context A was cleaned with a 0.5% hydrogen peroxide solution (Virox, Oakville, Canada) between each trial. Context B was a chamber of the same dimensions within a room with dim lighting. The chamber had a white plastic floor, curved white plastic walls, dim lighting, no background fan noise, and was scented with 0.25 % benzaldehyde in 70 % ethanol. Context B was cleaned with a 70 % ethanol solution between each trial. On day 7, mice were allowed to explore context A for 4 min. At 180 s, white noise (85 dB) played for 30 s and was co-terminated with a foot shock (2 s, 0.75 mA). After the 4-min trial, the mouse was returned to its home cage. On day 8, mice were allowed to explore context A for 4 min in the absence of white noise and foot shock (context recall). On day 9, mice were allowed to explore context B in the constant presence of white noise (85 dB, cue recall). For all tasks, the behavior was analyzed and recorded with Any-Maze v6.0 (Stoelting, Wood Dale, IL).

## Tissue Preparation

For brain collection, mice from all groups were perfused after behavioral tests. The brain tissues, which were randomly chosen, were dissected into the cerebral cortex (CTX) and the other hemisphere for molecular experiments, including RNA sequencing, RT-qPCR, and western blot. The brain tissue from the remaining mice was fixed with 4% paraformaldehyde (PFA) for 24 h for immunohistochemistry. All samples were stored at  $-80^{\circ}\text{C}$  or  $4^{\circ}\text{C}$  before further analysis.

## Immunohistochemistry

After completion of behavioral studies, a subset of mice was deeply anesthetized with ketamine/xylazine (100 mg/kg + 10 mg/kg, intraperitoneally), and then perfused transcardially with cold sterile PBS followed by 4 % PFA in PBS. Brains were removed, drop-fixed in 4 % PFA overnight, then washed once with cold PBS and stored in PBS. Tissue sections (50  $\mu\text{m}$  thick) were taken with a vibratome (Leica; Wetzlar, Germany) and were stored in PBS with 0.02 % sodium azide (w/v). Sections were washed in PBS followed by 10-min permeabilization in 0.1 % Triton X-100 in PBS (PBST). Sections were then incubated in blocking solution (5 % normal goat serum in PBST) for 1.5 h. The sections were washed three times with PBST and incubated with primary antibodies diluted in blocking solution: 1:500 rabbit anti-Iba1 (ab178846, Abcam) and 1:250 chicken anti-GFP (A10262, ThermoFisher) overnight at  $4^{\circ}\text{C}$ . Post incubation, the sections were washed three times in PBST and incubated with secondary antibodies diluted in blocking solution for 2 h at room temperature (RT): goat anti-rabbit conjugated Alexa Fluor 568 (Abcam #175471, 1:500) and 1:500 goat anti-chicken Alexa Fluor 488 (A11039, Thermo Fisher). The sections were washed three times in PBST and incubated in 1  $\mu\text{M}$  DAPI solution (#ab228549, Abcam) for 5 min. The sections were washed twice in PBS and mounted on slides using ProLong Diamond Antifade Mountant (P36970, Thermo Fisher).

## Stereology and Cell Morphology

Assessment of neuronal loss was assessed by GFP-expressing neuron count and roundness in the layers IV and V of the primary somatosensory (S1) cortex. Similarly, microglia density was determined in the same layers IV and V of the S1 cortical region by MBF stereo investigator (Williston VT). The number of sections required for brain region was determined by an initial pilot study which found that six sections were needed for the S1 cortical region, each spaced equidistantly for both GFP-expressing neurons and Iba-1 immunopositive microglia. A widefield microscope (AxioImager M2/Z2, Carl Zeiss, Oberkochen, Germany) along with MBF

stereo investigator was used to visualize each section and to determine the number of microglia in brain region. Using the optical fractionator workflow, the region of interest was traced onto each section based on the mouse brain atlas by Paxinos and Franklin. This was followed by a systematically random grid overlay consisting of squares measuring 300  $\mu\text{m}$  by 300  $\mu\text{m}$ , covering the region of interest. From each of these squares, an unbiased sampling region (100  $\mu\text{m}$  by 100  $\mu\text{m}$ ) was used to manually count microglia somata in the area. Once each section was completed, the software ran an algorithm to estimate the number of microglia in the region. In parallel for Iba-1 immunopositive microglia, the Cavalieri estimator in the software was used to determine the volume of brain region. The microglia count and volume were then used to determine the microglia density in the S1 cortical region. For assessment of cell morphology, images of coronal sections were taken on a Zeiss LSM880 Airyscan confocal microscope (Oberkochen, Germany) using an X20/0.8 NA air immersion objective controlled by the Zeiss Zen Black software. For 3D analysis, z-stack images were obtained by capturing an image every 0.7  $\mu\text{m}$  covering the entire 50- $\mu\text{m}$ -thick section. Images were deconvoluted using AutoQuant X3.1 (Media Cybernetics, Rockville, MD) and 3D analysis was performed using Imaris 9.1.2 (Bit Plane Inc., Concord, MA) using the surface tool to reconstruct the soma and the filament tool to reconstruct the branches.

### Western Blotting

After completion of behavioral trials, a subset of mice was sacrificed and brain regions were immediately frozen on dry ice. Cerebral cortex was lysed with 1X cell lysis buffer supplemented with 1 mM PMSF (Cell Signaling #8553S, Danvers, MA) and protease inhibitor cocktail (Sigma-Aldrich #11873580001). Tissue lysates were separated by electrophoresis and then transferred to a nitrocellulose membrane. Membranes were blocked for 1 h at RT, followed by treatment with primary antibodies (anti-caspase-1 antibody, 20B-0042; anti-IL-1 $\beta$  antibody 6243S; anti-NLRP3 antibody, AG-20B-0014-C100; anti-ASC antibody, AG-25B-0006-C100; anti- $\alpha$ -tubulin antibody, T9026) at 4°C for overnight. Each membrane was then treated with a secondary antibody conjugated with horseradish peroxidase (anti-rabbit-or anti-mouse IgG-HRP-antibodies) for 1h at RT. Each band was detected using chemiluminescence detection kit (32106; Thermo Fisher Scientific) and data was analyzed using the Image J software to measure relative protein expression.

### Cortical Microglia Cultures

Cortices from 1-3-day-old C57BL/6J mouse pups were isolated, digested, and seeded at a density of 8 cortices per 24-well plate (12 mL total volume). Every 3 days, the

medium (DMEM + 10 % FBS + 1 % penicillin-streptomycin) was replenished. After 3 weeks, mixed glial cultures reached confluence and were isolated by mild trypsinization as previously described [18]. Briefly, cells were washed with culture medium without FBS and treated with a mixture of trypsin (0.25 % without EDTA) and DMEM-F12 medium in a 1:3 ratio. After 40-min incubation, mixed glial cells detached and left a layer of microglia attached to the bottom of the culture dish. Pure microglia were isolated by 15-min incubation with trypsin (0.05% with EDTA) at 37°C followed by gentle shaking. Cells were counted and seeded in 24-well plates at a density of  $7.5 \times 10^4$  cells/well.

### Cortical Neuron Cultures

Cortices from 3-day-old C57BL/6J mouse pups were isolated and finely diced in ice-cold HBSS. Cortices were then incubated in 10X trypsin solution (Sigma #59427C) with DNase I (Sigma #D4513) for 15 min at 37 °C with period inversion. Cells were then spun at 200 g for 5 min, and the pellet was triturated with a serological pipette and strained in a 40- $\mu\text{m}$  cell strainer (BD Falcon #352340). Centrifugation followed by trituration was repeated once, and then the pellet was spun down and resuspended in neurobasal medium supplemented with 0.25 % GlutaMAX, 2 % B-27, 10 % fetal bovine serum, and 1 % penicillin/streptomycin at a density of  $5 \times 10^5$  cell/mL. Two hours later, the medium was changed to neurobasal medium supplemented with 0.25 % GlutaMAX, 2 % B-27, and 1 % penicillin/streptomycin, and half the medium was replenished every 3-4 days afterward. Three days later, cells were infected with  $2 \times 10^{10}$  vg/mL AAV. Expression was confirmed by fluorescence microscopy. Cell supernatant and lysates were collected for assessment of LDH release and CXCL10 production (R&D Systems #DY466).

### Analysis of Cytokines

IL-1 $\beta$  in microglia culture supernatant was measured with Mouse IL-1 $\beta$  /IL-1F2 DuoSet ELISA Kit (R&D Systems DY401, Minneapolis, MN) according to the manufacturer's instructions. CXCL10 was measured in neuronal culture supernatant with Mouse CXCL10 DuoSet ELISA (R&D Systems DY466-05, Minneapolis, MN) according to the manufacturer's instructions. Primary microglia were stimulated with recombinant Mouse CXCL10 protein (R&D Systems 466-CR-608 050/CF, Minneapolis, MN) and incubated with Mouse CXCL10 antibody (R&D Systems AF-466-609 NA, Minneapolis, MN). TNF- $\alpha$  and IL-1 $\beta$  were measured in the supernatant by ELISA with Mouse TNF- $\alpha$  Quantikine ELISA Kit (R&D Systems MTA00B, Minneapolis, MN) and Mouse IL-1 $\beta$ /IL-1F2 DuoSet ELISA Kit according to manufacturer's instructions.

## Gene Expression and RNAseq

Total RNA was isolated using the RNeasy Minikit (QIAGEN #74106; Hilden, Germany) and precipitated by the ethanol/sodium acetate method. RNA concentration and quality were initially measured using a Nanodrop 2000 (Thermo Fisher). Secondary analysis of concentration and quality was conducted by the Genomics CoRE Facility at the Icahn School of Medicine at Mount Sinai using Qubit RNA BR Assay Kit (ThermoFisher #Q10211). Library construction and RNA sequencing were performed by Novogene (Durham, NC). RNAseq data were processed using the NGS-Data-Charmer pipeline. Briefly, adaptors and low-quality bases were trimmed from reads, which were then aligned to the mm10 genome using HISAT2 (version 2.2.1). Read counts in the mm10 GENCODE annotation (version M22) were generated using FeatureCounts DESeq2 (version 1.24.0, R version 3.6.1) and then used to calculate differential expression from the read counts. The R package “biomaRt” (version 2.40.5) was used to translate ensembl ids into common gene symbols.

## Gene Ontology

Mouse genes involved in inflammatory processes were extracted from the Mouse Genome Informatics (MGI) group database. MGI mouse genes with the GO term “inflammatory response” were extracted. Ingenuity pathway analysis was applied to all differential genes identified in the previous analysis.

## Quantitative Reverse Transcription PCR

For qPCR analysis, gene expression was measured in 4 replicates by Power UP SYBR Green Master Mix (Thermo Fisher #A25778) using an ABI PRISM 7900HT Sequence Detection System. Hypoxanthine phosphoribosyl transferase (*Hprt*) expression level was used as an internal control and data was normalized using the  $2^{-\Delta\Delta C_t}$  method [19]. Levels of target gene mRNA were expressed relative to those of GFP + Veh mice for in vivo studies. Primers used in this study were designed using the Primer-BLAST software [20] and are listed in Supplementary Table S1.

## Statistical Analysis

All figure values are presented as the mean and standard error of the mean (S.E.M). Statistical tests are indicated in the figure legends. A confidence interval of 95 % was used for all analyses. In all studies, outliers (> 2 SD from the mean) were excluded. All statistical analyses were performed using the GraphPad Prism 9 software (GraphPad Software, San Diego, CA). \* $p < 0.05$ , \*\* $p < 0.01$ ,

\*\*\* $p < 0.001$ , \*\*\*\* $p < 0.0001$ , *ns* not significant. Statistically insignificant trends are indicated by *p*-value.

## Results

### GFP-(GR)<sub>100</sub> Animal Model of C9orf72 FTD/ALS Exhibits Behavioral Impairment, Neurodegeneration, and Neuroinflammation, Leading to a Significant Innate Immune-Driven Response

To investigate the effects of GR<sub>100</sub>-induced neuronal stress in the brain in *C9orf72* FTD/ALS, neonatal intracerebroventricular injections of adeno-associated virus serotype 9 (AAV<sub>9</sub>) vectors containing either GFP (control) or 100 repeats of the GR dipeptide (GFP-(GR)<sub>100</sub>) were conducted, as previously reported [21]. AAV<sub>9</sub> has a strong expression pattern in neurons of the brain, but not microglia [22], allowing for the targeted investigation of neuronal-induced effects. The body weight of GFP and GFP-(GR)<sub>100</sub> mice did not differ throughout the study (Supplementary Fig. 1a). Examination of *C9orf72* FTD/ALS behavioral features in GFP-(GR)<sub>100</sub> revealed significant mortality over the course of 3 months after injection, with over 25 % of animals dying before completion (Fig. 1b). To assess behavioral responses, mice were tested for contextual memory, motor function, and anxiety. GFP-(GR)<sub>100</sub> animals exhibited a significant reduction in freezing in the contextual memory paradigms (\*\* $p < 0.01$ , Fig. 1c), as well as a significant increase in falls in the hanging wire test (\*\*\*\* $p < 0.0001$ , Fig. 1d). Similarly, GFP-(GR)<sub>100</sub> mice exhibited a significant elevated anxiety in the open field test (\* $p < 0.05$ , Fig. 1e).

Next, cortical neuron degeneration was assessed by quantification of GFP-expressing neurons in the layers of IV and V in the S1 cortical region, which revealed a significant reduction in GFP-expressing neurons in GFP-(GR)<sub>100</sub> mice, indicative of neurodegeneration (\*\*\* $p < 0.001$ , lower left panel of Fig. 1f). GFP-(GR)<sub>100</sub> and GFP exhibit a cytoplasmic distribution in all neurons; therefore, we utilized the GFP tag as a maker to assess neuronal morphology and found neurons in the S1 cortical region revealing a significant increase in somatic roundness (\*\*\*\* $p < 0.0001$ , lower right panel of Fig. 1f), a measure of cellular atrophy, corresponding to neuronal injury and axonal degeneration [23].

Microglia-mediated neuroinflammation has been described in cases of ALS [24]. Microgliosis has also been previously described to occur in this model, beginning at 1.5 months of age [25]. We hypothesized that microglia, the innate immune cells of the brain, may be causally related to the pathogenesis of *C9orf72* FTD/ALS. To determine microglial response to the disease process, we first stereologically quantified the density of microglia in the S1, a

relevant region of the brain that contributes to the behavioral impairments we observed in GFP-(GR)<sub>100</sub> (upper panel of Fig. 1g). We found a significant increase of microglia density in GFP-(GR)<sub>100</sub> mice compared to GFP mice (\*  $p < 0.05$ , Fig. 1h). Moreover, morphological analyses were conducted to assess activation state of microglia (middle and lower panels of Fig. 1g), which revealed a trending increase in the level of ramifications closer to the soma in GFP-(GR)<sub>100</sub> mice as reflected by the increase in intersecting segments within 10  $\mu\text{m}$  of the soma compared to GFP mice. This is accompanied by a statistically significant decrease in the number of intersecting segments further away from the soma (20–30  $\mu\text{m}$  away from the soma) as assessed by Sholl analysis, indicative of an activated state with increased branch complexity (\*\* $p < 0.001$ , Fig. 1i). This increased density and morphological ramification of microglia is indicative of a neuroinflammatory response occurring in the S1 cortical regionally overlapping neuronal loss in GFP-(GR)<sub>100</sub> mice.

Next, we investigated the effects of microglial activation seen in GFP-(GR)<sub>100</sub> mice in neuroinflammatory responses as assessed by innate immunity including cleavage of caspase-1, IL-1 $\beta$ , NLRP3, and ASC protein level (Fig. 1j–m). Interestingly, we found that GFP-(GR)<sub>100</sub> mice exhibited an increase in the ratio of active caspase-1 to pro-caspase-1 (\*\* $p < 0.01$ , Fig. 1j) in the cerebral cortex. As expected, IL-1 $\beta$  was significantly increased in the same brain region of GFP-(GR)<sub>100</sub> compared to GFP mice (\* $p < 0.05$ , Fig. 1k). GFP-(GR)<sub>100</sub> mice also revealed a trend of elevation of NLRP3 and ASC protein expression compared to GFP mice (Fig. 1l and 1m). Collectively, the elevation of active caspase-1, IL-1 $\beta$ , and activation of microglia suggests that there is a significant innate immune-driven response in vivo in GFP-(GR)<sub>100</sub> mice potentially associated with activation of inflammasome in microglia.

### Genetic Ablation of Nlrp3 Inflammasome Confers Protection Against Innate Immune-Driven Inflammation in the Cerebral Cortex of C9orf72 FTD/ALS Mice

Based upon our results identifying significant innate immune-related inflammation in a GFP-(GR)<sub>100</sub> model of C9orf72 FTD/ALS, we targeted the NLRP3 inflammasome complex via genetic ablation. To test the effects of genetic ablation of *Nlrp3*, GFP-(GR)<sub>100</sub>, or GFP expression in the mouse brain, we conducted neonatal intracerebroventricular injections of AAV<sub>9</sub> vectors in mice lacking the *Nlrp3* gene (*Nlrp3*<sup>-/-</sup>).

Weights of *Nlrp3*<sup>-/-</sup>-GFP and *Nlrp3*<sup>-/-</sup>-GFP-(GR)<sub>100</sub> did not differ over the course of the study (Supplementary Fig. 1b). Next, examination of the behavioral effects of inflammasome targeted interventions revealed no change in mortality in *Nlrp3*<sup>-/-</sup>-GFP-(GR)<sub>100</sub> mice compared to *Nlrp3*<sup>-/-</sup>-GFP mice (Fig. 2a). Assessment of memory

function demonstrated unaffected contextual memory in *Nlrp3*<sup>-/-</sup>-GFP-(GR)<sub>100</sub> mice compared to *Nlrp3*<sup>-/-</sup>-GFP mice (Fig. 2b). Similarly, motor function (Fig. 2c) and anxiety (Fig. 2d) assessed by hanging wire and open field tests remained unaffected in *Nlrp3*<sup>-/-</sup>-GFP-(GR)<sub>100</sub>, with mice equally performing as found in *Nlrp3*<sup>-/-</sup>-GFP mice.

We next investigated the effects of targeting the NLRP3 inflammasome on neurodegeneration in GFP-(GR)<sub>100</sub> mice in the S1 cortical region. No changes in both neuronal count and somatic roundness of GFP-expressing neurons were found in *Nlrp3*<sup>-/-</sup>-GFP-(GR)<sub>100</sub> compared to *Nlrp3*<sup>-/-</sup>-GFP (Fig. 2e). This evidence tentatively suggests a causal effect between *Nlrp3* silencing and lack of neurodegeneration and behavioral impairments.

Based on our evidence of inflammasome-mediated neuroinflammation in the cerebral cortex of WT GFP-(GR)<sub>100</sub> mice (Fig. 1j and 1m), we further investigated these findings in the cerebral cortex of *Nlrp3*<sup>-/-</sup>-GFP-(GR)<sub>100</sub> mice. We found no change in the ratio active caspase-1 to pro-caspase-1 in *Nlrp3*<sup>-/-</sup>-GFP-(GR)<sub>100</sub> mice compared to *Nlrp3*<sup>-/-</sup>-GFP mice (Fig. 2f). Similarly, no significant differences in level of active IL-1 $\beta$  were observed in *Nlrp3*<sup>-/-</sup>-GFP-(GR)<sub>100</sub> mice compared to *Nlrp3*<sup>-/-</sup>-GFP mice (Fig. 2g). We also verified genotype of *Nlrp3*<sup>-/-</sup> mice which were confirmed with PCR genotyping (Fig. 2h). This evidence supports hypothesis of microglia-driven innate immune responses in the brain of C9orf72 FTD/ALS.

### GFP-(GR)<sub>100</sub> Expression Induces Transcriptional Changes in Innate Immune Microglia-Mediated Responses of C9orf72 FTD/ALS Mice

We next investigated the transcriptional regulation of genes in the CTX of GFP-(GR)<sub>100</sub> mice relative to GFP mice to assess regional distribution of changes. Overall transcriptional patterns depicting the significantly differentially expressed genes are visualized in Fig. 3a, with the top three mapped upregulated and downregulated genes labeled as identified by the magnitude of log<sub>2</sub>fold change, as visualized in a volcano plot. The top-upregulated mapped gene in GFP-(GR)<sub>100</sub> is *Cxcl10* (log<sub>2</sub>fold change = 4.51;  $p_{\text{adj}} = 0.06$ , Fig. 3a), which has been previously shown to result in the proliferation and activation of microglia [26]. Based on this in vivo data suggesting a causal link between inflammasome activation and neurodegeneration resulting in behavioral impairments, we hypothesized that GFP-(GR)<sub>100</sub> expression would invoke transcriptional changes in innate immune responses. Functional prediction analysis was assessed by ingenuity pathway analysis (IPA) using significant differentially expressed genes. Our analysis revealed that several neuroinflammatory signaling pathways, including the “complement system,” “TREM1 signaling,” “chemokine signaling,” and “NF- $\kappa$ B signaling,” were enriched in the CTX of

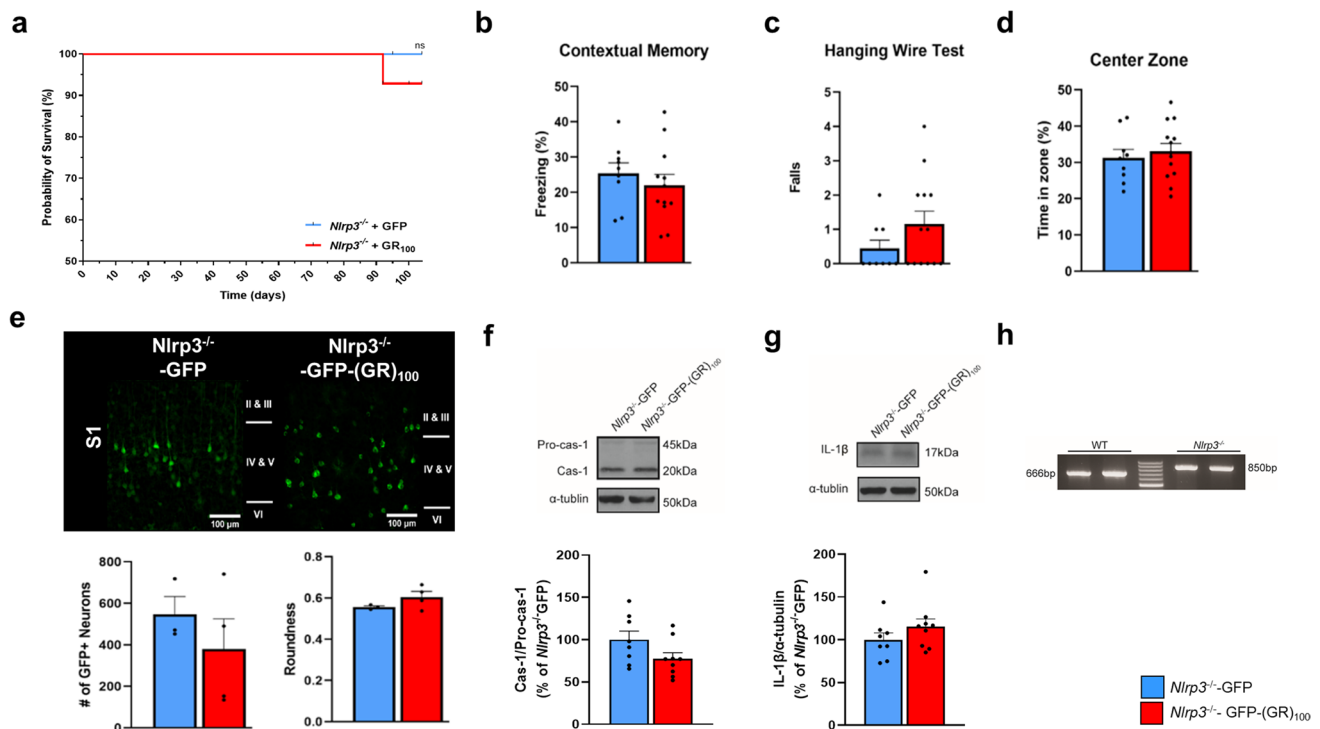


**Fig. 2** Attenuation of neurodegeneration and behavioral deficits caused by genetic ablation of *Nlrp3*<sup>-/-</sup> in a GFP-(GR)<sub>100</sub> model of *C9orf72* FTD/ALS. **a** Probability of survival of *Nlrp3*<sup>-/-</sup>-GFP and *Nlrp3*<sup>-/-</sup>-GFP-(GR)<sub>100</sub> mice. The probability of survival was analyzed by log-rank test. **b** Freezing in contextual fear memory task. **c** Number of falls in the third day of the hanging wire test. **d** Time spent in the center zone in the open field test ( $n=9$ – $12$  mice for each group). **e** Representative *Nlrp3*<sup>-/-</sup>-GFP and *Nlrp3*<sup>-/-</sup>-GFP-(GR)<sub>100</sub> expressing neurons in the layers IV and V of S1 cortical region, green: GFP and GFP-(GR)<sub>100</sub>. Length bar, 100  $\mu$ m. Bar graph showing the count (lower left panel) and somatic roundness (lower right panel) of *Nlrp3*<sup>-/-</sup>-GFP- and *Nlrp3*<sup>-/-</sup>-GFP-(GR)<sub>100</sub>-expression neu-

rons in the layers IV and V of S1 cortical region ( $n=3$ – $4$  mice for each group). **f** Representative bands (upper panel) and densitometric quantification of the ratio of active caspase-1 to pro-caspase-1 (lower panel) in the cerebral cortex, normalized to GFP mice. **g** Representative bands (upper panel) and densitometric quantification of the ratio of cleaved IL-1 $\beta$  caspase-1 to  $\alpha$ -tubulin (lower panel) in the cerebral cortex, normalized to *Nlrp3*<sup>-/-</sup>-GFP mice ( $n=7$ – $8$  mice for each group). **h** Representative image showing PCR products with a band at 850 bp for *Nlrp3*<sup>-/-</sup> mice and a band at 666 bp for WT mice. **b**–**g** were analyzed by unpaired *t*-test. Data are presented as mean  $\pm$  SEM

GFP-(GR)<sub>100</sub> mice. These pathways are core regulators of inflammatory responses and microglial activation. Amongst validated genes (Fig. 3c), we found that *Cxcl10* is significantly upregulated, with a 3.5-fold increase in GFP-(GR)<sub>100</sub> mice, compared to GFP mice ( $***p < 0.001$  Fig. 3d). The transcriptomic changes exhibited in GFP-(GR)<sub>100</sub> animals heavily point to significant innate immune microglia-mediated responses. Our findings of significant *Cxcl10* upregulation suggest there is a neuronal signal released that can activate microglia and induce innate immune cascades in GFP-(GR)<sub>100</sub> mice.

### GFP-(GR)<sub>100</sub> Induces Secretion of Neuronal CXCL10 Activating a Microglial Innate Immune Response

As *Cxcl10* is an important signal for the immune responses of microglia [26], we investigated the effect of GFP-(GR)<sub>100</sub> infection in primary neuronal and microglial cultures on

CXCL10 production, and whether CXCL10 induces microglia activation. First, we investigated whether the expression of GFP-(GR)<sub>100</sub> induced neuronal cell death in vitro. GFP-(GR)<sub>100</sub> transfected neurons exhibited a significant increase in the release of lactate dehydrogenase (LDH) compared to GFP transfected neurons ( $*p < 0.05$ , Fig. 4a), confirming the GFP-(GR)<sub>100</sub>-induced neuronal injury and death observed in vivo. As *Cxcl10* was shown to be highly upregulated in vivo in GFP-(GR)<sub>100</sub> mice, we hypothesized that neurons are able to produce and secrete CXCL10, in response to GFP-(GR)<sub>100</sub>. To test this, primary cortical neurons were transfected with either AAV<sub>9</sub>-GFP or AAV<sub>9</sub>-GR<sub>100</sub> and cell supernatants were analyzed for CXCL10 concentration. GFP-(GR)<sub>100</sub> neurons demonstrated significantly increased production of CXCL10 compared to GFP transfected neurons ( $***p < 0.0001$ , Fig. 4b). As we identified *Cxcl10* is highly upregulated in vivo and was determined experimentally to be significantly released by primary cortical



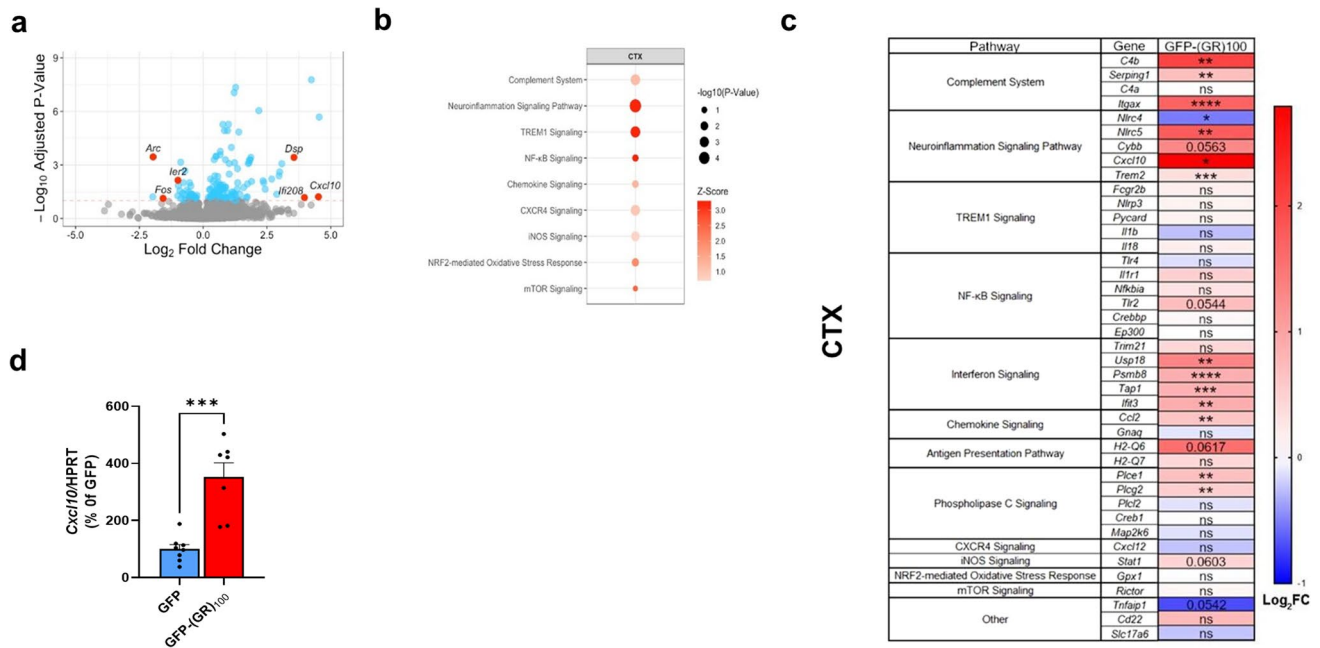


**Fig. 3** Transcriptional changes of GFP-(GR)<sub>100</sub>. **a** A volcano plot of cerebral cortex (CTX) transcription. The X-axis represents the log<sub>2</sub> fold change, while the Y-axis represents the negative log<sub>10</sub> FDR-adjusted *p*-value. Genes with an adjusted *p*-value less than 0.10 are shown in blue. The 3 most highly upregulated mapped genes and 3 most highly downregulated genes are highlighted in red. **b** Inflammation-related IPA pathway; select immune system-related pathways are shown for the CTX. The *p*-value of each entry is represented by the size of the corresponding circle. The *z*-score, indicating the computed activation or repression of the given pathway, is indicated

with a color gradient. **c** Validation of significant IPA genes identified via RNAseq. Gene ontologies are indicated on the left. Colors indicate log<sub>2</sub> fold change (\**p* < 0.05, \*\**p* < 0.01, \*\*\**p* < 0.001, \*\*\*\**p* < 0.0001, *p* < 0.1; statistically insignificant trends, *p* > 0.1; ns; not significant, *n* = 4 mice for each group). **d** Validation of the most highly upregulated gene, *Cxcl10* mRNA expression, in the CTX of GFP and GFP-(GR)<sub>100</sub> mice (\*\*\**p* < 0.001, compared to GFP mice, *n* = 7–8 mice for each group). **c–d** were analyzed by two-tailed Welch's *t*-test. Data are presented as mean ± SEM

GFP-(GR)<sub>100</sub> neurons in vitro, we next investigated whether CXCL10 activates microglia.

Tumor necrosis factor- $\alpha$  (TNF- $\alpha$ ) constitutes a hallmark for microglia activation and has previously been shown to play an important role in the transcriptional regulation of components of the NLRP3 inflammasome [27]. To test the ability of CXCL10 to induce TNF- $\alpha$  expression, primary cortical microglia cultures were treated with increasing CXCL10 concentration and assessed released level of TNF- $\alpha$  in cell supernatant. We found that CXCL10 significantly increased the microglial production of TNF- $\alpha$  in a dose-dependent manner (\*\**p* < 0.01; \*\*\*\**p* < 0.0001, Fig. 4c), while the co-treatment with a CXCL10 neutralizing antibody results in a significant reduction in the TNF- $\alpha$  secreted by microglia (\*\*\*\**p* < 0.0001, Fig. 4d). Finally, we assessed whether CXCL10 mediates the activation of inflammasome complexes involved in IL-1 $\beta$  processing by measuring the release of IL-1 $\beta$  from primary cortical microglia in response to increasing concentrations of CXCL10. Our results showed a significant and dose-dependent increase in the secretion of IL-1 $\beta$  in response to CXCL10 at concentrations of 50–100 ng/mL (\*\*\*\**p* < 0.0001, Fig. 4e). Co-treatment with CXCL10 neutralizing antibody results in a significant reduction in IL-1 $\beta$  released by microglia (\*\**p* <

0.01; \*\*\**p* < 0.001; \*\*\*\**p* < 0.0001, Fig. 4f). This evidence suggests neuronal-microglial crosstalk whereby GFP-(GR)<sub>100</sub> induces secretion of neuronal CXCL10, activating a microglial innate immune response, resulting in inflammasome activation and subsequent neuroinflammation.

In conjunction with the rest of our data, these experiments suggest that neurons in *C9orf72* FTD/ALS produce damage-associated molecular patterns (DAMPs) such as CXCL10 caused by GFP-(GR)<sub>100</sub>, which significantly stimulates pro-inflammatory reactions from microglia, leading to inflammasome activation (Fig. 4g).

## Discussion

Our study provides evidence linking inflammasome activation to neurodegeneration and provides a basis for the investigation of innate immune inflammasome inhibitors as a treatment of disease in *C9orf72* FTD/ALS. Here, we identify a key mechanism by which neuronal stress initiated by G<sub>4</sub>C<sub>2</sub> HREs in *C9orf72* FTD/ALS can activate microglia, producing an inflammasome-dependent innate immune response, which can be therapeutically targeted. As

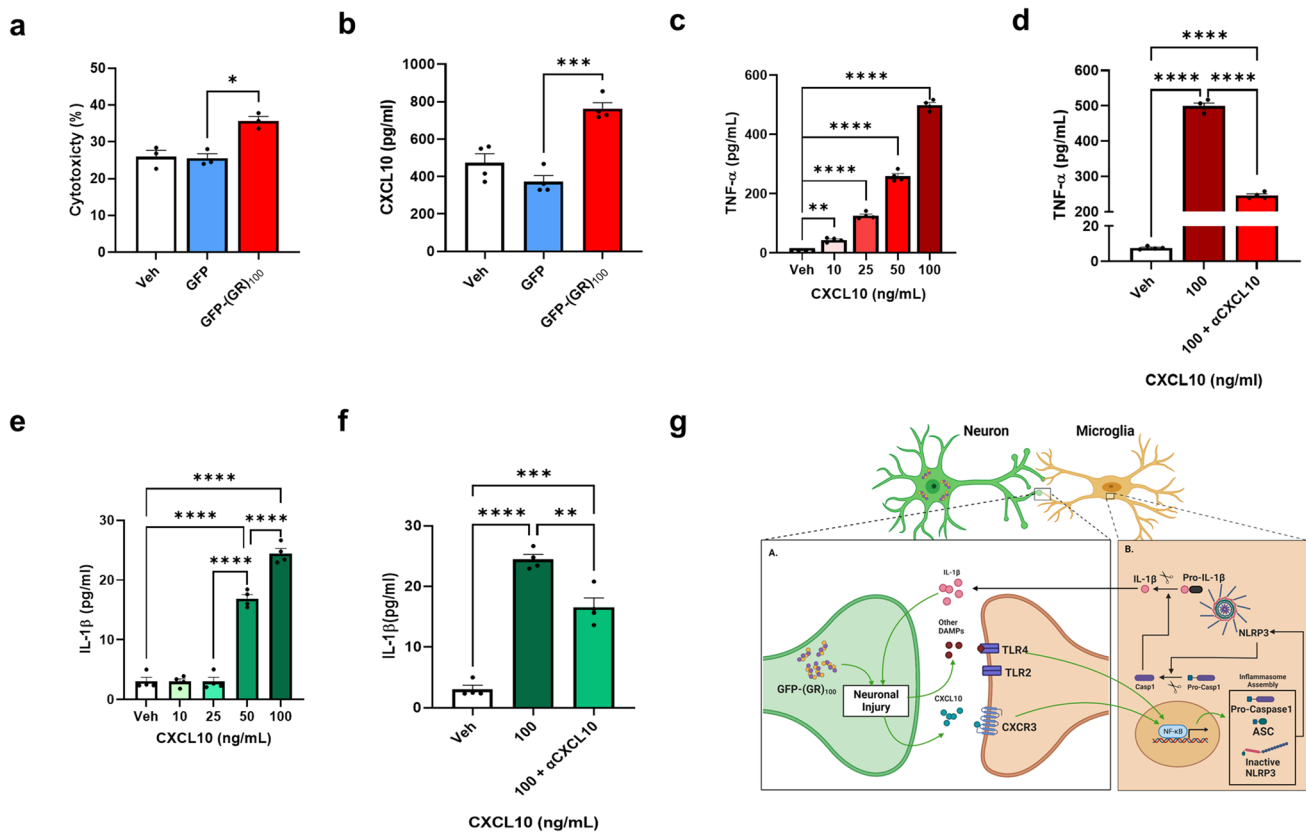


**Fig. 4** In vitro evaluation of neuronal signaling and resultant activation microglia in *C9orf72* FTD/ALS. **a** Evaluation of neurotoxicity of GFP-(GR)<sub>100</sub>. **b** Neuronal release of CXCL10 after transfection with GFP-(GR)<sub>100</sub>. **c** CXCL10-mediated dose-dependent release of TNF-α. **d** Neutralization of CXCL10 and the release of TNF-α. **e** CXCL10-mediated dose-dependent release of IL-1β. **f** Neutralization of CXCL10 and IL-1β release. **g** Schematized mechanism

of GFP-(GR)<sub>100</sub> inducing the neuronal release of CXCL10, which may then bind to microglial receptors and initiate an inflammasome response. The data shown correspond to average values of biological triplicates ran in technical duplicates. **a-f** were analyzed by one-way ANOVA (\* $p < 0.05$ , \*\* $p < 0.01$ , \*\*\* $p < 0.001$ , \*\*\*\* $p < 0.0001$  compared to vehicle,  $n = 3-4$  mice for each group). Data are presented as mean  $\pm$  SEM

neuronal stress occurs throughout various forms of FTD/ALS [28–30], the self-perpetuating cycle of neuronal stress inducing microglial inflammasome activation and resultant neuroinflammation may represent a conserved therapeutic substrate throughout the various disease subtypes of FTD/ALS. Ultimately, we demonstrate that by targeting microglial reactivity through inflammasome inhibition, FTD/ALS pathogenesis was significantly attenuated through the genetic ablation of *Nlrp3*.

The results of these studies identify the contributions of inflammasome activation in microglia to the pathogenesis of *C9orf72* FTD/ALS. Microglial activation and the activation of the NLRP3 inflammasome have been demonstrated as crucial mediators in other neurodegenerative conditions including Alzheimer's disease (AD) [21], Parkinson's disease (PD) [31], and primary progressive multiple sclerosis [32]. Inflammation has also been noted pre-symptomatically in models of ALS [33, 34] and the incidence of ALS has been demonstrated to be higher in individuals who have

been diagnosed with autoimmune disease [35], indicating a putative role in the disease pathogenesis and a target for therapeutic intervention. Neuroimaging studies conducted on individuals with ALS have demonstrated microglial activation throughout the brain [24, 36].

Upon examination of the microglia in the S1 cortical region, we observed microgliosis consistent with previously identified findings [25]. Morphologically, microglia in GFP-(GR)<sub>100</sub> were in an activated state; these findings are congruent with those identified in other neurodegenerative diseases, including AD, in which morphologically activated microglia are present [37]. Inflammasome activation has been identified in other forms of ALS [38–40]. We noted an increase in the ratio of active caspase-1 to pro-caspase-1 in the CTX of WT GFP-(GR)<sub>100</sub> mice; these increases were attenuated via genetic ablation of *Nlrp3* as well as the production of active IL-1β. These results shed light on the role the NLRP3 inflammasome might have on the pathogenesis of FTD/ALS.

In addition to improvements in neurodegeneration and neuroinflammation, full genetic ablation of the *Nlrp3*<sup>-/-</sup> inflammasome conferred significant protection behaviorally in *Nlrp3*<sup>-/-</sup>-GFP-(GR)<sub>100</sub> mice compared to *Nlrp3*<sup>-/-</sup>-GFP mice; mortality was almost completely eliminated, contextual memory was preserved, motor function was protected, and no increase in anxiety was observed. To determine if the NLRP3 inflammasome can be therapeutically targeted, further studies may employ experimental models whereby *Nlrp3* ablation in microglia by Cre-dependent designer receptor exclusively activated by designer drugs (DREADD) mice allow for temporal control of *Nlrp3* expression. Additionally, future studies can expand on the current in vivo and in vitro evidence by examining the mechanisms including translocation of NF-κB and the activation of the inflammasome. This approach can evaluate the role of NLRP3 inflammasome in pre-symptomatic disease and determine whether it can be a viable therapeutic target after symptom onset.

*Cxcl10*, which we found to be highly upregulated in the cerebral cortex of GFP-(GR)<sub>100</sub> mice, encodes for a small cytokine belonging to the CXC chemokine family. Upon neuronal death, CXCL10 is produced and exerts a chemotactic function by attracting microglia and CD8<sup>+</sup> T cells, and can induce the activation of microglia, thereby causing the release of pro-inflammatory cytokines [41]. Chemotactic effects are demonstrated in our FTD/ALS model by the microgliosis in the cortex of GFP-(GR)<sub>100</sub> mice where we see a significant increase in the density of microglia. Neuronal stress has been demonstrated in other forms of ALS, including in cases of sporadic ALS [42]. Dysregulation of CXCL10 chemotaxis in peripheral blood cells from ALS patients has been directly observed, which was associated with increased inflammatory responses [43]. This evidence supports our in vitro findings, where we demonstrated that neuronal cultures expressing (GR)<sub>100</sub> dipeptides released higher concentrations of CXCL10, and the treatment of microglia cultures with increasing concentrations of CXCL10 promoted a dose-dependent increase in TNF-α and IL-1β production indicating microglial activation.

In summary, our studies identify a novel neuronal-microglial crosstalk mechanism in *C9orf72* FTD/ALS whereby neuronal stress-induced secretion of CXCL10 triggers inflammasome activation in microglia, thereby creating a self-propagating cycle of neurodegeneration and neuroinflammation. Our findings show targeting the inflammasome responses represents a putative therapeutic strategy, as evidenced by the genetic ablation of *Nlrp3* and resultant protection from behavioral impairment and neuropathology.

**Supplementary Information** The online version contains supplementary material available at <https://doi.org/10.1007/s12035-023-03315-w>.

**Acknowledgements** We thank Josh Palmieri for his impeccable work with administrative duties.

**Author Contribution** K.J.T and E.Y conducted in vivo experiments of the GFP-(GR)<sub>100</sub> model. Immunofluorescence staining, image acquisition, and analysis were performed by K.J.T, C.S, U.H.I, U.R, and T.O. In vitro experiments were conducted by M.S.V, M.A.R, and R.I.A. Molecular analyses, including western blots, and RT-qPCR were performed by K.J.T, C.S, E.Y, M.S.V., H.W, and M.A.R. Bioinformatics analyses were conducted by H.W and M.E. Generation and purification of the GFP-(GR)<sub>100</sub> and GFP viruses were completed by Y.J.Z and L.P. K.J.T, C.S, F.J.H, and G.M.P designed the project. K.J.T, E.Y, C.S, R.I.A, and G.M.P prepared the manuscript. All authors discussed and commented on the article.

**Funding** The study was supported by the generous support of the Altschul Foundation to G.M.P. and by the Veteran Administration program on ALS. G.M.P. holds a Senior VA Career Scientist Award. We acknowledge that the contents of this study do not represent the views of the NCCIH, the ODS, the National Institutes of Health, the US Department of Veterans Affairs, or the United States Government.

**Data availability** The authors declare that the data supporting the findings of this study are available within the paper and its supplementary information files. Any remaining data that support the results of the study will be available from the corresponding author upon reasonable request.

## Declarations

**Ethics Approval** All of the experimental procedures were approved by the Mount Sinai Institutional Animal Care and Use Committee (IACUC) (approval number: IACUC-2019-0006).

**Consent to Participate** Not applicable.

**Consent for Publication** Not applicable.

**Competing Interests** The authors declare no competing interests.

## References

1. Hardiman O, Al-Chalabi A, Chio A, Corr EM, Logroscino G, Robberecht W, Shaw PJ, Simmons Z et al (2017) Amyotrophic lateral sclerosis. *Nat Rev Dis Primers* 3:17071. <https://doi.org/10.1038/nrdp.2017.71>
2. Renton AE, Majounie E, Waite A, Simon-Sanchez J, Rollinson S, Gibbs JR, Schymick JC, Laaksovirta H et al (2011) A hexanucleotide repeat expansion in C9ORF72 is the cause of chromosome 9p21-linked ALS-FTD. *Neuron* 72(2):257–268. <https://doi.org/10.1016/j.neuron.2011.09.010>
3. DeJesus-Hernandez M, Mackenzie IR, Boeve BF, Boxer AL, Baker M, Rutherford NJ, Nicholson AM, Finch NA et al (2011) Expanded GGGGCC hexanucleotide repeat in noncoding region of C9ORF72 causes chromosome 9p-linked FTD and ALS. *Neuron* 72(2):245–256. <https://doi.org/10.1016/j.neuron.2011.09.011>
4. Sakae N, Bieniek KF, Zhang YJ, Ross K, Gendron TF, Murray ME, Rademakers R, Petrucelli L et al (2018) Poly-GR dipeptide repeat polymers correlate with neurodegeneration and clinicopathological subtypes in C9ORF72-related brain disease. *Acta Neuropathol Commun* 6(1):63. <https://doi.org/10.1186/s40478-018-0564-7>
5. Chew J, Cook C, Gendron TF, Jansen-West K, Del Rosso G, Daugherty LM, Castanedes-Casey M, Kurti A et al (2019) Aberrant deposition of stress granule-resident proteins linked to

- C9orf72-associated TDP-43 proteinopathy. *Mol Neurodegener* 14(1):9. <https://doi.org/10.1186/s13024-019-0310-z>
6. Krishnan G, Raitcheva D, Bartlett D, Prudencio M, McKenna-Yasek DM, Douthwright C, Oskarsson BE, Ladha S et al (2022) Poly(GR) and poly(GA) in cerebrospinal fluid as potential biomarkers for C9ORF72-ALS/FTD. *Nat Commun* 13(1):2799. <https://doi.org/10.1038/s41467-022-30387-4>
  7. Gascon E, Gao FB (2014) The emerging roles of microRNAs in the pathogenesis of frontotemporal dementia-amyotrophic lateral sclerosis (FTD-ALS) spectrum disorders. *J Neurogenet* 28(1–2):30–40. <https://doi.org/10.3109/01677063.2013.876021>
  8. Moisse K, Strong MJ (2006) Innate immunity in amyotrophic lateral sclerosis. *Biochim Biophys Acta* 1762(11–12):1083–1093. <https://doi.org/10.1016/j.bbadis.2006.03.001>
  9. Trageser KJ, Smith C, Herman FJ, Ono K, Pasinetti GM (2019) Mechanisms of immune activation by c9orf72-expansions in amyotrophic lateral sclerosis and frontotemporal dementia. *Front Neurosci* 13:1298. <https://doi.org/10.3389/fnins.2019.01298>
  10. Ising C, Heneka MT (2018) Functional and structural damage of neurons by innate immune mechanisms during neurodegeneration. *Cell Death Dis* 9(2):120. <https://doi.org/10.1038/s41419-017-0153-x>
  11. Herman FJ, Pasinetti GM (2018) Principles of inflammasome priming and inhibition: Implications for psychiatric disorders. *Brain Behav Immun* 73:66–84. <https://doi.org/10.1016/j.bbi.2018.06.010>
  12. Freeman L, Guo H, David CN, Brickey WJ, Jha S, Ting JP (2017) NLR members NLRC4 and NLRP3 mediate sterile inflammasome activation in microglia and astrocytes. *J Exp Med* 214(5):1351–1370. <https://doi.org/10.1084/jem.20150237>
  13. Zhu LY, Liu C, Li ZR, Niu C, Wu J (2021) NLRP3 deficiency did not attenuate NASH development under high fat calorie diet plus high fructose and glucose in drinking water. *Lab Invest* 101(5):588–599. <https://doi.org/10.1038/s41374-021-00535-3>
  14. Glascock JJ, Osman EY, Coady TH, Rose FF, Shababi M, Lorton CL (2011) Delivery of therapeutic agents through intracerebroventricular (ICV) and intravenous (IV) injection in mice. *J Vis Exp* (56). <https://doi.org/10.3791/2968>
  15. Cook C, Petrucelli L (2019) Genetic convergence brings clarity to the enigmatic red line in ALS. *Neuron* 101(6):1057–1069. <https://doi.org/10.1016/j.neuron.2019.02.032>
  16. Seibenhener ML, Wooten MC (2015) Use of the Open Field Maze to measure locomotor and anxiety-like behavior in mice. *J Vis Exp* (96):e52434. <https://doi.org/10.3791/52434>
  17. Aartsma-Rus A, van Putten M (2014) Assessing functional performance in the mdx mouse model. *J Vis Exp* (85). <https://doi.org/10.3791/51303>
  18. Saura J, Tusell JM, Serratos J (2003) High-yield isolation of murine microglia by mild trypsinization. *Glia* 44(3):183–189. <https://doi.org/10.1002/glia.10274>
  19. Livak KJ, Schmittgen TD (2001) Analysis of relative gene expression data using real-time quantitative PCR and the 2<sup>-</sup>(delta delta C(T)) method. *Methods* 25(4):402–408. <https://doi.org/10.1006/meth.2001.1262>
  20. Ye J, Coulouris G, Zaretskaya I, Cutcutache I, Rozen S, Madden TL (2012) Primer-BLAST: a tool to design target-specific primers for polymerase chain reaction. *BMC Bioinformatics* 13:134. <https://doi.org/10.1186/1471-2105-13-134>
  21. Heneka MT, Kummer MP, Stutz A, Delekate A, Schwartz S, Vieira-Saecker A, Griep A, Axt D et al (2013) NLRP3 is activated in Alzheimer's disease and contributes to pathology in APP/PS1 mice. *Nature* 493(7434):674–678. <https://doi.org/10.1038/nature11729>
  22. Su W, Kang J, Sopher B, Gillespie J, Aloï MS, Odum GL, Hopkins S, Case A et al (2016) Recombinant adeno-associated viral (rAAV) vectors mediate efficient gene transduction in cultured neonatal and adult microglia. *J Neurochem* 136(Suppl 1):49–62. <https://doi.org/10.1111/jnc.13081>
  23. Lacroix A, Toussay X, Anenberg E, Lecrux C, Ferreiros N, Karagiannis A, Plaisier F, Chausson P et al (2015) COX-2-derived prostaglandin E2 produced by pyramidal neurons contributes to neurovascular coupling in the rodent cerebral cortex. *J Neurosci* 35(34):11791–11810. <https://doi.org/10.1523/JNEUROSCI.0651-15.2015>
  24. Corcia P, Tauber C, Vercoullie J, Arlicot N, Prunier C, Praline J, Nicolas G, Venel Y et al (2012) Molecular imaging of microglial activation in amyotrophic lateral sclerosis. *PLoS One* 7(12):e52941. <https://doi.org/10.1371/journal.pone.0052941>
  25. Zhang YJ, Gendron TF, Ebbert MTW, O'Raw AD, Yue M, Jansen-West K, Zhang X, Prudencio M et al (2018) Poly(GR) impairs protein translation and stress granule dynamics in C9orf72-associated frontotemporal dementia and amyotrophic lateral sclerosis. *Nat Med* 24(8):1136–1142. <https://doi.org/10.1038/s41591-018-0071-1>
  26. Clarner T, Janssen K, Nellessen L, Stangel M, Skripuletz T, Krauspe B, Hess FM, Denecke B et al (2015) CXCL10 triggers early microglial activation in the cuprizone model. *J Immunol* 194(7):3400–3413. <https://doi.org/10.4049/jimmunol.1401459>
  27. McGeough MD, Wree A, Inzaugarat ME, Haimovich A, Johnson CD, Pena CA, Goldbach-Mansky R, Broderick L et al (2017) TNF regulates transcription of NLRP3 inflammasome components and inflammatory molecules in cryopyrinopathies. *J Clin Invest* 127(12):4488–4497. <https://doi.org/10.1172/JCI90699>
  28. Zhang X, Wang F, Hu Y, Chen R, Meng D, Guo L, Lv H, Guan J et al (2020) In vivo stress granule misprocessing evidenced in a FUS knock-in ALS mouse model. *Brain* 143(5):1350–1367. <https://doi.org/10.1093/brain/awaa076>
  29. Peters OM, Ghasemi M, Brown RH Jr (2015) Emerging mechanisms of molecular pathology in ALS. *J Clin Invest* 125(5):1767–1779. <https://doi.org/10.1172/JCI71601>
  30. Thonhoff JR, Simpson EP, Appel SH (2018) Neuroinflammatory mechanisms in amyotrophic lateral sclerosis pathogenesis. *Curr Opin Neurol* 31(5):635–639. <https://doi.org/10.1097/WCO.0000000000000599>
  31. Fan Z, Pan YT, Zhang ZY, Yang H, Yu SY, Zheng Y, Ma JH, Wang XM (2020) Systemic activation of NLRP3 inflammasome and plasma alpha-synuclein levels are correlated with motor severity and progression in Parkinson's disease. *J Neuroinflammation* 17(1):11. <https://doi.org/10.1186/s12974-019-1670-6>
  32. Malhotra S, Costa C, Eixarch H, Keller CW, Amman L, Martinez-Banaclocha H, Midaglia L, Sarro E et al (2020) NLRP3 inflammasome as prognostic factor and therapeutic target in primary progressive multiple sclerosis patients. *Brain* 143(5):1414–1430. <https://doi.org/10.1093/brain/awaa084>
  33. Sanagi T, Yuasa S, Nakamura Y, Suzuki E, Aoki M, Warita H, Itoyama Y, Uchino S et al (2010) Appearance of phagocytic microglia adjacent to motoneurons in spinal cord tissue from a presymptomatic transgenic rat model of amyotrophic lateral sclerosis. *J Neurosci Res* 88(12):2736–2746. <https://doi.org/10.1002/jnr.22424>
  34. Wang R, Yang B, Zhang D (2011) Activation of interferon signaling pathways in spinal cord astrocytes from an ALS mouse model. *Glia* 59(6):946–958. <https://doi.org/10.1002/glia.21167>
  35. Turner MR, Goldacre R, Ramagopalan S, Talbot K, Goldacre MJ (2013) Autoimmune disease preceding amyotrophic lateral sclerosis: an epidemiologic study. *Neurology* 81(14):1222–1225. <https://doi.org/10.1212/WNL.0b013e3182a6cc13>
  36. Turner MR, Cagnin A, Turkheimer FE, Miller CC, Shaw CE, Brooks DJ, Leigh PN, Banati RB (2004) Evidence of widespread cerebral microglial activation in amyotrophic lateral sclerosis: an [11C](R)-PK11195 positron emission tomography study. *Neurobiol Dis* 15(3):601–609. <https://doi.org/10.1016/j.nbd.2003.12.012>
  37. Baron R, Babcock AA, Nemirovsky A, Finsen B, Monsonego A (2014) Accelerated microglial pathology is associated with Abeta plaques in mouse models of Alzheimer's disease. *Aging Cell* 13(4):584–595. <https://doi.org/10.1111/acel.12210>

38. Debye B, Schmulling L, Zhou L, Rune G, Beyer C, Johann S (2018) Neurodegeneration and NLRP3 inflammasome expression in the anterior thalamus of SOD1(G93A) ALS mice. *Brain Pathol* 28(1):14–27. <https://doi.org/10.1111/bpa.12467>
39. Moreno-Garcia L, Miana-Mena FJ, Moreno-Martinez L, de la Torre M, Lunetta C, Tarlarini C, Zaragoza P, Calvo AC et al (2021) Inflammasome in ALS skeletal muscle: NLRP3 as a potential biomarker. *Int J Mol Sci* 22(5). <https://doi.org/10.3390/ijms22052523>
40. Johann S, Heitzer M, Kanagaratnam M, Goswami A, Rizo T, Weis J, Troost D, Beyer C (2015) NLRP3 inflammasome is expressed by astrocytes in the SOD1 mouse model of ALS and in human sporadic ALS patients. *Glia* 63(12):2260–2273. <https://doi.org/10.1002/glia.22891>
41. Klein RS, Lin E, Zhang B, Luster AD, Tollett J, Samuel MA, Engle M, Diamond MS (2005) Neuronal CXCL10 directs CD8+ T-cell recruitment and control of West Nile virus encephalitis. *J Virol* 79(17):11457–11466. <https://doi.org/10.1128/JVI.79.17.11457-11466.2005>
42. Sasaki S (2010) Endoplasmic reticulum stress in motor neurons of the spinal cord in sporadic amyotrophic lateral sclerosis. *J Neuro-pathol Exp Neurol* 69(4):346–355. <https://doi.org/10.1097/NEN.0b013e3181d44992>
43. Perner C, Perner F, Stubendorff B, Forster M, Witte OW, Heide F, Prell T, Grosskreutz J (2018) Dysregulation of chemokine receptor expression and function in leukocytes from ALS patients. *J Neuroinflammation* 15(1):99. <https://doi.org/10.1186/s12974-018-1135-3>

**Publisher's Note** Springer Nature remains neutral with regard to jurisdictional claims in published maps and institutional affiliations.